IEEE Access
Multidisciplinary | Rapid Review | Open Access Journal

Received 10 January 2023, accepted 19 January 2023, date of publication 30 January 2023, date of current version 9 February 2023.

Digital Object Identifier 10.1109/ACCESS.2023.3240506

RESEARCH ARTICLE

A Virtual Full-Duplex Relaying Scheme and Adjustment Algorithms for Enhancing Spectral Efficiency in UAV-Aided Communication Networks

DONG HYUCK WOO[1] AND HO YOUNG HWANG[2], (Member, IEEE)
[1]Department of Computer Engineering, Kwangwoon University, Seoul 01897, Republic of Korea
[2]School of Computer and Information Engineering, Kwangwoon University, Seoul 01897, Republic of Korea

Corresponding author: Ho Young Hwang (hyhwang@kw.ac.kr)

This work was supported in part by the Basic Science Research Program through the National Research Foundation of Korea (NRF) funded by the Ministry of Education under Grant NRF-2018R1D1A1B07049601, and in part by the Research Grant of Kwangwoon University, in 2021.

ABSTRACT Utilizing unmanned aerial vehicles (UAVs) as relays has great potential owing to their high mobility in communication networks. To fully exploit this mobility characteristic, we propose a UAV-aided relaying scheme with a data ferrying protocol. By employing two UAVs, our proposed relaying scheme performs virtual full-duplex (FD) transmission to increase the end-to-end spectral efficiency (SE) performance. To further enhance the performance, we propose a center point adjustment algorithm and a transmit power adjustment algorithm. We evaluate the performance of our proposed adjustment algorithms by comparing the relaying schemes with and without the proposed adjustment algorithms. Simulation results show that our proposed relaying scheme with our proposed adjustment algorithms can achieve higher SE performance compared to conventional schemes.

INDEX TERMS UAV, relay, virtual full-duplex, spectral efficiency.

I. INTRODUCTION

Relaying has been extensively studied owing to its various advantages in communication networks. Relaying is a communication technique in which the relay assists in transmitting the source's information to the destination and has advantages, such as coverage extension, path loss reduction, and increased end-to-end performance [1], [2], [3]. Recently, relaying has attracted attention owing to its utility in various technologies, such as cognitive radio (CR), non-orthogonal multiple access (NOMA), and device-to-device (D2D); furthermore, it can satisfy the demand for coverage extension when using mmWave in 5G [3], [4], [5], [6]. Relaying techniques such as half-duplex (HD), full-duplex (FD), and virtual FD have been proposed, depending on the transmittance and reception of data. For HD systems [7], [8], [9], data transmission and data reception are performed separately by dividing time and frequency resources, and various relay selection schemes have been proposed to enhance the end-to-end performance [8], [9]. Because the relay selection schemes in [8] and [9] use buffers, transmitting data immediately after reception is not essential, thereby increasing diversity and end-to-end performance. However, despite various relay selection schemes, HD has low spectral efficiency (SE) owing to the pre-log factor caused by dividing resources. For FD systems, data transmission and data reception are simultaneously performed at the same time and frequency. This simultaneous transmission and reception causes self-interference (SI), and studies have been performed to reduce SI [10], [11], [12]. However, it is difficult to completely remove SI owing to the high power of the signal transmitted from the relay itself [5]. Additionally, practical application of FD is difficult because of its expensiveness and complexity [13]. For virtual FD systems, mimicking FD, data transmission and data reception

The associate editor coordinating the review of this manuscript and approving it for publication was Tariq Umer.

are performed simultaneously to enhance the SE, whereas the transmission and reception are performed separately by different relays to avoid SI. Compared to SI, the occurrence of inter-relay interference (IRI) is easier to prevent because the separation distance between antennas is greater than that in FD [14]. Regarding studies on virtual FD, such as [15], successive relaying (SuR) was proposed that involves two relays, each of which transmits or receives data alternatively. Additionally, numerous relay selection schemes using buffers have been proposed [16], [17], [18]. In [16], SFD-MMRS scheme was proposed, which selects two relays that configure the best source-relay and relay-destination links, respectively, based on signal-to-noise ratio (SNR). In [17], a relay selection scheme named BA-SOR was proposed, which considers IRI. Hence, a relay that configures the source-relay link is selected based on the ratio of the transmitted signal power to the interference signal power. In BA-SOR, an interference cancellation (IC) technique that removes interference larger than a certain intensity was considered. In [18], two relay selection schemes were proposed to enhance the sum-throughput. An optimization process for the transmit power and relay selection was performed under the transmit power limit and minimum required rate.

A. RELATED WORKS AND MOTIVATIONS

Recently, studies have been performed on the utilization of UAVs as relays [19], [20] because of the reduced cost of a UAV [3], [21] and compared to a conventional ground relay, using a UAV is advantageous owing to its mobility. These studies can be classified based on the method used to transmit and receive data. In [22], when an HD relay (UAV) moves along a circular trajectory, transmission time and transmission power are optimized to minimize the outage probability. This process was performed in the Rayleigh channel and Rician channel. In [21], when a UAV performs FD relaying, its transmission power and trajectory were optimized to maximize the system throughput. In [23], by employing the SuR scheme in a UAV-aided relay system, the minimum rate obtained by the user is maximized using power allocation and relay selection. Additionally, IRI caused by simultaneous transmissions was considered.

Various studies consider data ferrying and relaying in combination when a UAV has a storage cache, such as a buffer, and is employed in a delay-tolerant environment [24], [25], [26], [27], [28]. Studies combining data ferrying and HD relaying have been conducted [25], [26], [27]. In [25], for the circular motion of UAV, the transmission time is divided using the time-division duplex (TDD), and the UAV receives and stores data from the source node for a certain period of time, and then transmits the data to the destination node. The transmission time and trajectory were jointly optimized to maximize SE and energy efficiency (EE). In [26], the TDD mode is adopted similar to [25] such that a UAV can collect data from the source and forward the collected data to the destination in the presence of an eavesdropper. The communication scheduling, transmit power, and trajectory of the UAV were jointly optimized to maximize the secrecy energy efficiency (SEE). In [27], for the rectilinear motion of UAV, a multicasting scenario was considered in which the UAV receives data from a base station, carries it for a certain distance, and transmits the same data to multiple receivers. To optimize EE and reliability, the energy minimization and outage minimization problems were solved by considering the data ferrying distance. In [28], the data ferrying technique was merged with a FD relaying system. When a UAV moves rectilinearly, the transmission phase is divided into two phases, in each of which the UAV performs FD relaying. The objective was to enhance the EE by considering the motional speed of the UAV. To the best of our knowledge, no studies have combined data ferrying and virtual FD relaying for the case of two UAVs used as relays moving along a circular trajectory.

B. CONTRIBUTIONS

In this paper, a virtual FD relaying scheme with data ferrying is proposed to enhance the system SE. Virtual FD relaying simultaneously transmits and receives data; thus, it can have a higher SE than HD relaying. Additionally, virtual FD relaying prevents the SI occurring in FD relaying because transmission and reception are performed by different relays. Additionally, for data ferrying, SE can be increased by reducing the path loss between the transmitting and receiving nodes. The main contributions of this study are as follows:

- A relaying scheme that employs a virtual FD protocol and a data ferry is proposed to enhance the SE in UAV-aided communication networks.
- To increase the end-to-end performance, methods for adjusting the transmission power and center point of the trajectory are proposed. By differentiating the SNR and signal-to-interference-plus-noise ratio (SINR) with respect to the transmission power and center point of the trajectory, the corresponding variables are adjusted.
- The simulation results show the effect of adjusting the transmission power and center point of the trajectory in relaying systems. Furthermore, the performance of the proposed relaying scheme exhibits a higher SE compared to the conventional relaying schemes.

The remainder of this paper is organized as follows. In Section II, the system model is presented. In Section III, our proposed relaying scheme is introduced. In Section IV, methods are presented for adjusting the transmission power and center point of the trajectory to increase the performance of our proposed relaying scheme. In Section V, simulation results are presented to evaluate the performance of our proposed relaying scheme using two of the proposed adjustment methods. Finally, Section VI, concludes the paper. Additionally, the main notations are given in Table 1.

TABLE 1. Notations.

Notation	Meaning
S	Source node
D	Destination node
R_i	i-th relay node (UAV), $i \in \{1, 2\}$
v	Velocity of the UAV
H	Height of the UAV
C	Center of the trajectory
r	Radius of the trajectory
T	Period
$\mathbf{X}_i$	Position of node i
x_i	x coordinate of node i
θ_i	Angle between R_i and the y-axis
β	Channel power at a reference distance
λ	Wavelength
$\|\cdot\|$	2-norm distance
α	Path loss exponent
P_S	Transmit power of the source node
P_{R_2}	Transmit power of the UAV
σ^2	Noise power

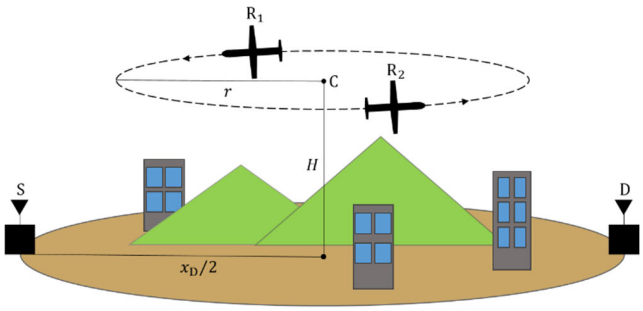

FIGURE 1. Illustration of a UAV-aided communication network.

II. SYSTEM MODEL

We consider a downlink UAV-aided communication network in which UAVs are used as relays. As shown in Fig. 1, there is a source node S, destination node D, and UAVs R_1 and R_2, each containing a single antenna; thus, the HD mode can be performed. The UAVs follow an energy-efficient circular trajectory [25] at a velocity of v and height H. The UAVs act as decode-and-forward (DF) relays; thus, each UAV that has received data from S decodes and stores the data and then, forwards the data to D. The center and radius of the trajectory are denoted as C and r, respectively, and the UAVs are assumed to rotate counterclockwise. The period T required for the UAV to complete one round of the trajectory can be represented as $T = 2\pi r/v$. Without loss of generality, we consider the Cartesian coordinates. The positions of S, D, and C can be represented as $\mathbf{X}_S = (0, 0, 0)$, $\mathbf{X}_D = (x_D, 0, 0)$, and $\mathbf{X}_C = (x_C, 0, H)$, respectively. As shown in Fig. 1, we assume that $r \leq x_D/2$ and C is initially located in the middle of S and D, i.e., $x_C^{\text{initial}} = x_D/2$. If we assume that the two UAVs R_i, $i = \{1, 2\}$ have moved for t seconds ($0 \leq t \leq T$), the position of R_i can be represented as $\mathbf{X}_{R_i}(x_C, \theta_i(t)) = (x_C - r\sin\theta_i(t), r\cos\theta_i(t), H)$, where $\theta_i(t) = \theta_i(0) + vt/r$. $\theta_i(t)$ represents the angle between R_i and the y-axis at time t. It is assumed that the direct communication between S and D is negligible owing to the severe path loss caused by long distances and obstacles [14], [22], [26], [29], [30]. Thus, communication between S and D is assumed to be possible only via the UAVs. Accordingly, the ground-to-ground communication link between S and D is not configured, and each ground node can configure a line-of-sight (LOS) link with each aerial UAV. We assume that the Doppler effect can be ignored [21], [22]. Thus, a channel model can follow a free-space path loss model, and the channel gain between node i and node j can be represented as

$$g_{ij} = \beta \left\| \mathbf{X}_i - \mathbf{X}_j \right\|^{-\alpha} \tag{1}$$

where β is the channel power at a reference distance of 1 m, i.e., $\beta = (\lambda/4\pi)^2$; λ is the wavelength; $\mathbf{X}_i$ and $\mathbf{X}_j$ correspond to the positions of nodes i and j, respectively; $\|\cdot\|$ denotes the 2-norm distance; α is the path-loss exponent and $\alpha = 2$.

III. PROPOSED SCHEME

To enhance the performance of a UAV-aided relaying system, we propose a scheme that considers virtual FD and data ferrying in combination. Virtual FD can overcome the constraints of HD by mimicking the FD. In this study, we apply the SuR scheme [15] to our proposed scheme as a virtual FD.

Fig. 2 (a) shows the SuR scheme using two relays. The total operating time can be divided into slot units, and communication can be performed by dividing the slots into odd and even. The SuR scheme can proceed as follows: In the odd slot, R_1 can receive data from S and R_2 can transmit data to D simultaneously. Excluding the first slot, R_2 can transmit data received from S in the previous even slot to D. In the even slot, R_2 can receive data from S and R_1 can transmit data to D simultaneously. That is, in each slot excluding the first slot, by utilizing two relays, one relay can perform transmission while the other relay can perform reception in turn so that the reception of data and the transmission of data can be performed at the same time. Because the reception and transmission are performed simultaneously, as shown in Fig. 2 (a), IRI (dotted arrow) may occur in each slot; thus, it is difficult to achieve exactly twice the HD performance.

Fig. 2 (b) shows data ferrying using a moving UAV that relays data from S to D, each located terrestrially. From (1),

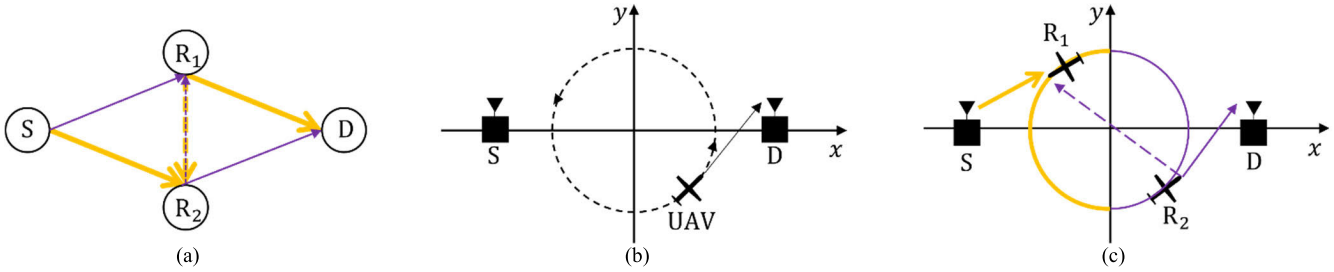

FIGURE 2. (a) Successive relaying (SuR); (b) Data ferrying; (c) The proposed relaying scheme.

small distance between a moving UAV and ground node corresponds to higher channel gain between them. Therefore, if a moving UAV communicates with a ground node closer to itself than the other ground node, a high channel gain between the UAV and the ground node can be obtained. To exploit this advantage, we adopt data ferrying using a moving UAV. If a moving UAV enters the vicinity of S, it receives and stores data from S until leaving its vicinity. Thereafter, the UAV reaches the vicinity of D and transmits the stored data until leaving its vicinity. Fig. 2 (b) shows the case where a UAV in the vicinity of D transmits data to D. To establish the criterion for determining the vicinity, we can use the distance between the UAV and each ground node, i.e., S and D. If $\|\mathbf{X}_S - \mathbf{X}_R\| < \|\mathbf{X}_R - \mathbf{X}_D\|$, then R is in the vicinity of S. If $\|\mathbf{X}_S - \mathbf{X}_R\| > \|\mathbf{X}_R - \mathbf{X}_D\|$, then R is in the vicinity of D.

Fig. 2 (c) shows the proposed scheme combining SuR with the data ferrying used herein. Our proposed scheme uses two moving UAVs to transmit and receive data simultaneously. The section in which each moving UAV communicates with a ground node can be adjusted using the above criterion. Thus, for a UAV located at $(0, r, H)$ to $(0, -r, H)$ and rotating counterclockwise along the trajectory, this section is defined as the $\{S \rightarrow R\}$ section where it communicates with S. If a UAV is located at $(0, -r, H)$ to $(0, r, H)$ and rotating counterclockwise along the trajectory, the corresponding section is defined as the $\{R \rightarrow D\}$ section where it communicates with D. Finally, we can set $\theta_1(0) = 0, \theta_2(0) = \pi$ and accordingly $\theta_1(t) = vt/r, \theta_2(t) = \pi + vt/r$.

As shown in Fig. 2 (c), let us define a UAV close to S as R_1 and a UAV close to D as R_2; therefore, R_1 is in the $\{S \rightarrow R\}$ section and R_2 is in the $\{R \rightarrow D\}$ section. Because two moving UAVs were considered, each UAV can alternate between the two sections. In $\{S \rightarrow R\}$ section, S and moving R_1 can configure a link at each instance, whereas in $\{R \rightarrow D\}$ section, moving R_2 and D can configure a link at each instance. Because R_1 and R_2 simultaneously transmit data and receive data, IRI can occur between R_1 and R_2, and a link between R_1 and R_2 can be configured. The channel gain in each link can be represented by, respectively,

$$g_{SR_1}(x_C, \theta_1) = \beta \left\| \mathbf{X}_S - \mathbf{X}_{R_1}(x_C, \theta_1) \right\|^{-\alpha} \quad (2a)$$

$$g_{R_2D}(x_C, \theta_2) = \beta \left\| \mathbf{X}_{R_2}(x_C, \theta_2) - \mathbf{X}_D \right\|^{-\alpha} \quad (2b)$$

$$g_{R_2R_1} = \beta (2r)^{-\alpha} \quad (2c)$$

Because the distance between R_1 and R_2 is $\left\| \mathbf{X}_{R_1} - \mathbf{X}_{R_2} \right\| = 2r$, the channel gain for IRI between R_1 and R_2 can be represented as (2c). Using (2), the instantaneous received SINR at R_1 in $\{S \rightarrow R_1\}$ link and at D in $\{R_2 \rightarrow D\}$ link are obtained by, respectively,

$$\gamma_{SR_1}(P_{R_2}, x_C, \theta_1) = \frac{P_S g_{SR_1}(x_C, \theta_1)}{\sigma^2 + P_{R_2} g_{R_2R_1}} \quad (3a)$$

$$\gamma_{R_2D}(P_{R_2}, x_C, \theta_2) = \frac{P_{R_2} g_{R_2D}(x_C, \theta_2)}{\sigma^2} \quad (3b)$$

where P_S is the transmission power of S, P_{R_2} is the transmission power of R_2, and σ^2 represents the power of additive white Gaussian noise (AWGN). Particularly, an IRI term appears in the denominator of (3a). According to (3), the SE of $\{S \rightarrow R_1\}$ link can be obtained using $SE_{SR_1}(P_{R_2}, x_C, \theta_1) = \log_2(1 + \gamma_{SR_1}(P_{R_2}, x_C, \theta_1))$ and the SE of $\{R_2 \rightarrow D\}$ link can be obtained using $SE_{R_2D}(P_{R_2}, x_C, \theta_2) = \log_2(1 + \gamma_{R_2D}(P_{R_2}, x_C, \theta_2))$. Finally, the average SE of $\{S \rightarrow R_1\}$ link and average SE of $\{R_2 \rightarrow D\}$ link can be represented as, respectively,

$$\begin{aligned}\overline{SE}_{SR_1}(P_{R_2}, x_C) &= \frac{1}{\pi}\int_0^{\pi} SE_{SR_1}(P_{R_2}, x_C, \theta_1)\, d\theta_1 \\ &= \frac{1}{\pi}\int_0^{\pi} \log_2(1 + \gamma_{SR_1}(P_{R_2}, x_C, \theta_1)) d\theta_1\end{aligned} \quad (4a)$$

$$\begin{aligned}\overline{SE}_{R_2D}(P_{R_2}, x_C) &= \frac{1}{\pi}\int_{\pi}^{2\pi} SE_{R_2D}(P_{R_2}, x_C, \theta_2)\, d\theta_2 \\ &= \frac{1}{\pi}\int_{\pi}^{2\pi} \log_2(1 + \gamma_{R_2D}(P_{R_2}, x_C, \theta_2)) d\theta_2\end{aligned} \quad (4b)$$

From (4) and information causality [30], the average end-to-end SE between S and D ($\overline{SE}_{SD}(P_{R_2}, x_C)$) is determined by the minimum value between $\overline{SE}_{SR_1}(P_{R_2}, x_C)$ and $\overline{SE}_{R_2D}(P_{R_2}, x_C)$.

$$\overline{SE}_{SD}(P_{R_2}, x_C) = \min\left(\overline{SE}_{SR_1}(P_{R_2}, x_C), \overline{SE}_{R_2D}(P_{R_2}, x_C)\right) \quad (5)$$

The next section discusses ways to increase $\overline{SE}_{SD}(P_{R_2}, x_C)$.

IV. ALGORITHMS FOR ENHANCING THE AVERAGE END-TO-END SE

In this system, from (5), $\overline{\mathrm{SE}}_{\mathrm{SD}}\left(P_{\mathrm{R}_2}, x_{\mathrm{C}}\right)$ is determined by the link with the lowest $\overline{\mathrm{SE}}$. If the minimum value between $\overline{\mathrm{SE}}_{\mathrm{SR}_1}\left(P_{\mathrm{R}_2}, x_{\mathrm{C}}\right)$ and $\overline{\mathrm{SE}}_{\mathrm{R}_2\mathrm{D}}\left(P_{\mathrm{R}_2}, x_{\mathrm{C}}\right)$ increases, then the average end-to-end SE ($\overline{\mathrm{SE}}_{\mathrm{SD}}\left(P_{\mathrm{R}_2}, x_{\mathrm{C}}\right)$) increases. Because $\overline{\mathrm{SE}}$ of each link can be represented by (4), we aim to improve the average end-to-end SE by adjusting the center of the UAV's trajectory (x_{C}) and the UAV's transmit power (P_{R_2}), which affect each link's $\overline{\mathrm{SE}}$.

A. CENTER POINT ADJUSTMENT ALGORITHM

In this subsection, a center point adjustment algorithm is proposed to improve $\overline{\mathrm{SE}}_{\mathrm{SD}}\left(P_{\mathrm{R}_2}, x_{\mathrm{C}}\right)$. We assume that P_{R_2} is given and the center point can be shifted along the x-axis. From Section II, the initial x_{C} is denoted as $x_{\mathrm{C}}^{\mathrm{initial}}$. The initial performances of each link, i.e., $\overline{\mathrm{SE}}_{\mathrm{SR}_1}\left(P_{\mathrm{R}_2}, x_{\mathrm{C}}^{\mathrm{initial}}\right)$ and $\overline{\mathrm{SE}}_{\mathrm{R}_2\mathrm{D}}\left(P_{\mathrm{R}_2}, x_{\mathrm{C}}^{\mathrm{initial}}\right)$, were compared and the x-axial movement direction of x_{C} was determined using the comparison results. The following three cases were obtained as the comparison results: 1. $\overline{\mathrm{SE}}_{\mathrm{SR}_1}\left(P_{\mathrm{R}_2}, x_{\mathrm{C}}^{\mathrm{initial}}\right) > \overline{\mathrm{SE}}_{\mathrm{R}_2\mathrm{D}}\left(P_{\mathrm{R}_2}, x_{\mathrm{C}}^{\mathrm{initial}}\right)$, 2. $\overline{\mathrm{SE}}_{\mathrm{SR}_1}\left(P_{\mathrm{R}_2}, x_{\mathrm{C}}^{\mathrm{initial}}\right) < \overline{\mathrm{SE}}_{\mathrm{R}_2\mathrm{D}}\left(P_{\mathrm{R}_2}, x_{\mathrm{C}}^{\mathrm{initial}}\right)$ 3. $\overline{\mathrm{SE}}_{\mathrm{SR}_1}\left(P_{\mathrm{R}_2}, x_{\mathrm{C}}^{\mathrm{initial}}\right) = \overline{\mathrm{SE}}_{\mathrm{R}_2\mathrm{D}}\left(P_{\mathrm{R}_2}, x_{\mathrm{C}}^{\mathrm{initial}}\right)$. Henceforth, we investigate the determination of x-axial movement direction of x_{C} and optimal x_{C} $\left(x_{\mathrm{C}}^{\mathrm{optimal}}\right)$ in Cases 1, 2, and 3.

1) CASE 1: $\overline{\mathrm{SE}}_{\mathrm{SR}_1}\left(P_{\mathrm{R}_2}, x_{\mathrm{C}}^{\mathrm{initial}}\right) > \overline{\mathrm{SE}}_{\mathrm{R}_2\mathrm{D}}\left(P_{\mathrm{R}_2}, x_{\mathrm{C}}^{\mathrm{initial}}\right)$

The x-axial movement direction of x_{C} is determined using the following proposition.

Proposition 1: $\overline{\mathrm{SE}}_{\mathrm{R}_2\mathrm{D}}\left(P_{\mathrm{R}_2}, x_{\mathrm{C}}\right)$ is monotonically increasing on $x_{\mathrm{C}} = (-\infty, x_{\mathrm{D}} - r]$, and monotonically decreasing on $x_{\mathrm{C}} = [x_{\mathrm{D}}, \infty)$. Additionally, $\overline{\mathrm{SE}}_{\mathrm{SR}_1}\left(P_{\mathrm{R}_2}, x_{\mathrm{C}}\right)$ is strictly decreasing on $x_{\mathrm{C}} = [x_{\mathrm{D}}/2, \infty)$.

Proof: See Appendix A.

From (5), $\overline{\mathrm{SE}}_{\mathrm{SD}}\left(P_{\mathrm{R}_2}, x_{\mathrm{C}}\right)$ is determined by the link with the lowest $\overline{\mathrm{SE}}$. Thus, $\overline{\mathrm{SE}}_{\mathrm{SD}}\left(P_{\mathrm{R}_2}, x_{\mathrm{C}}\right)$ increases as the minimum value between $\overline{\mathrm{SE}}_{\mathrm{SR}_1}\left(P_{\mathrm{R}_2}, x_{\mathrm{C}}\right)$ and $\overline{\mathrm{SE}}_{\mathrm{R}_2\mathrm{D}}\left(P_{\mathrm{R}_2}, x_{\mathrm{C}}\right)$ increases. As the constraint of $r \leq x_{\mathrm{D}}/2$, $x_{\mathrm{C}}^{\mathrm{initial}} (= x_{\mathrm{D}}/2)$ is less than or equal to $x_{\mathrm{D}} - r$, i.e., $x_{\mathrm{C}}^{\mathrm{initial}} \leq x_{\mathrm{D}} - r$. With the Proposition 1, $\overline{\mathrm{SE}}_{\mathrm{R}_2\mathrm{D}}\left(P_{\mathrm{R}_2}, x_{\mathrm{C}}\right)$ is monotonically increasing on $x_{\mathrm{C}} = (-\infty, x_{\mathrm{D}} - r]$. Thus, when $\overline{\mathrm{SE}}_{\mathrm{SR}_1}\left(P_{\mathrm{R}_2}, x_{\mathrm{C}}^{\mathrm{initial}}\right) > \overline{\mathrm{SE}}_{\mathrm{R}_2\mathrm{D}}\left(P_{\mathrm{R}_2}, x_{\mathrm{C}}^{\mathrm{initial}}\right)$, the x-axial movement direction of x_{C} is determined as the positive x-axis (D-side).

Furthermore, the distance moved by x_{C} to attain $x_{\mathrm{C}}^{\mathrm{optimal}}$ must be determined. Thus, as x_{C} moves toward D, the candidates for $x_{\mathrm{C}}^{\mathrm{optimal}}$ are explored. If there is no intersection between $\overline{\mathrm{SE}}_{\mathrm{SR}_1}\left(P_{\mathrm{R}_2}, x_{\mathrm{C}}\right)$ and $\overline{\mathrm{SE}}_{\mathrm{R}_2\mathrm{D}}\left(P_{\mathrm{R}_2}, x_{\mathrm{C}}\right)$ while moving x_{C} toward D, we only need to search x_{C} such that $\overline{\mathrm{SE}}_{\mathrm{R}_2\mathrm{D}}\left(P_{\mathrm{R}_2}, x_{\mathrm{C}}\right)$ has a local maximum (see Fig. 3 (a)). However, if there is an intersection between $\overline{\mathrm{SE}}_{\mathrm{SR}_1}\left(P_{\mathrm{R}_2}, x_{\mathrm{C}}\right)$ and $\overline{\mathrm{SE}}_{\mathrm{R}_2\mathrm{D}}\left(P_{\mathrm{R}_2}, x_{\mathrm{C}}\right)$ while moving x_{C} toward D, the x-coordinate of intersection may not be equal to $x_{\mathrm{C}}^{\mathrm{optimal}}$ (see Fig. 3 (b)), or it may be equal to $x_{\mathrm{C}}^{\mathrm{optimal}}$ (see Fig. 3 (c)). Thus, we consider x_{C} such that $\overline{\mathrm{SE}}_{\mathrm{R}_2\mathrm{D}}\left(P_{\mathrm{R}_2}, x_{\mathrm{C}}\right)$ has local maxima and x_{C} such that $\overline{\mathrm{SE}}_{\mathrm{SR}_1}\left(P_{\mathrm{R}_2}, x_{\mathrm{C}}\right)$ and $\overline{\mathrm{SE}}_{\mathrm{R}_2\mathrm{D}}\left(P_{\mathrm{R}_2}, x_{\mathrm{C}}\right)$ intersect as candidates. After completion of the search process, x_{C} having the highest $\overline{\mathrm{SE}}_{\mathrm{SD}}\left(P_{\mathrm{R}_2}, x_{\mathrm{C}}\right)$ among the candidates is determined as $x_{\mathrm{C}}^{\mathrm{optimal}}$.

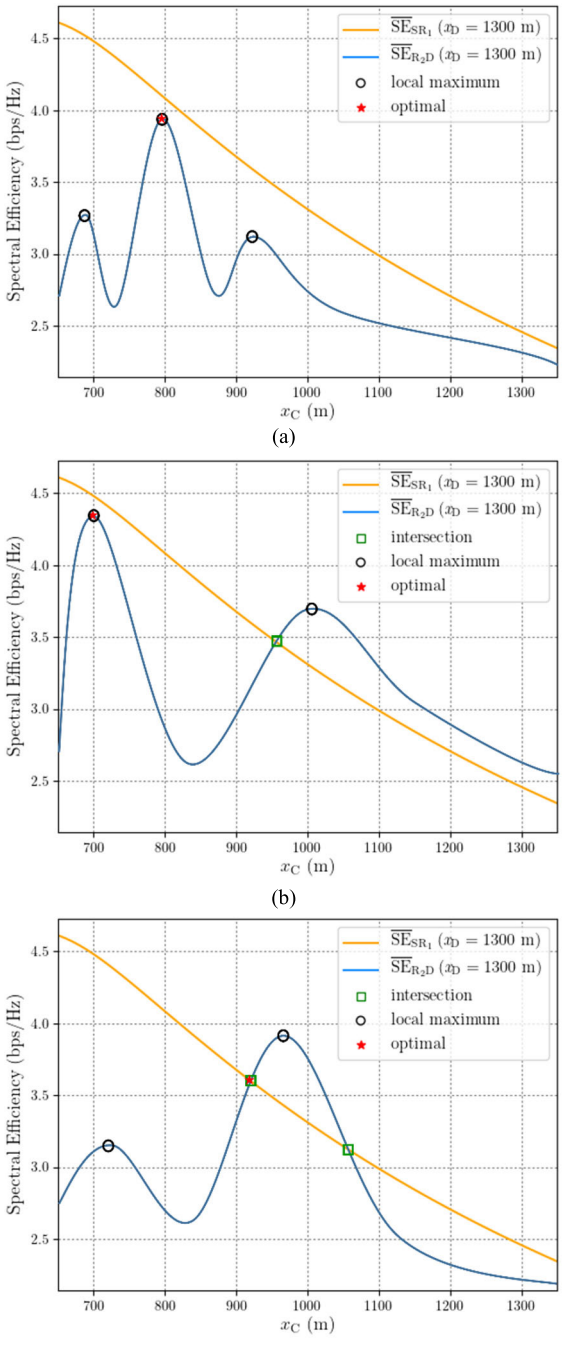

FIGURE 3. Examples of $\overline{\mathrm{SE}}_{\mathrm{SR}_1}$ and $\overline{\mathrm{SE}}_{\mathrm{R}_2\mathrm{D}}$ when $\overline{\mathrm{SE}}_{\mathrm{SR}_1}\left(P_{\mathrm{R}_2}, x_{\mathrm{C}}^{\mathrm{initial}}\right) > \overline{\mathrm{SE}}_{\mathrm{R}_2\mathrm{D}}\left(P_{\mathrm{R}_2}, x_{\mathrm{C}}^{\mathrm{initial}}\right)$. (a) The case that an intersection does not exist. (b) The case that an intersection exists and local maximum point is an optimal point. (c) The case that an intersection exists and the intersection is an optimal point.

2) CASE 2: $\overline{\mathrm{SE}}_{\mathrm{SR}_1}\left(P_{\mathrm{R}_2}, x_{\mathrm{C}}^{\mathrm{initial}}\right) < \overline{\mathrm{SE}}_{\mathrm{R}_2\mathrm{D}}\left(P_{\mathrm{R}_2}, x_{\mathrm{C}}^{\mathrm{initial}}\right)$

The x-axial movement direction of x_{C} is determined using the following proposition.

Proposition 2: $\overline{\mathrm{SE}}_{\mathrm{SR}_1}\left(P_{\mathrm{R}_2}, x_{\mathrm{C}}\right)$ is monotonically decreasing on $x_{\mathrm{C}} = [r, \infty)$ and monotonically increasing on $x_{\mathrm{C}} = (-\infty, 0]$. Additionally, $\overline{\mathrm{SE}}_{\mathrm{R}_2\mathrm{D}}\left(P_{\mathrm{R}_2}, x_{\mathrm{C}}\right)$ is strictly increasing on $x_{\mathrm{C}} = (-\infty, x_{\mathrm{D}}/2]$.

Proof: See Appendix B.

From (5), $\overline{\mathrm{SE}}_{\mathrm{SD}}\left(P_{\mathrm{R}_2}, x_{\mathrm{C}}\right)$ is determined by the link having the lowest $\overline{\mathrm{SE}}$. Thus, $\overline{\mathrm{SE}}_{\mathrm{SD}}\left(P_{\mathrm{R}_2}, x_{\mathrm{C}}\right)$ increases as the minimum value between $\overline{\mathrm{SE}}_{\mathrm{SR}_1}\left(P_{\mathrm{R}_2}, x_{\mathrm{C}}\right)$ and $\overline{\mathrm{SE}}_{\mathrm{R}_2\mathrm{D}}\left(P_{\mathrm{R}_2}, x_{\mathrm{C}}\right)$ increases. As the constraint of $r \leq x_{\mathrm{D}}/2$, $x_{\mathrm{C}}^{\mathrm{initial}} (= x_{\mathrm{D}}/2)$ is greater than or equal to r, i.e., $r \leq x_{\mathrm{C}}^{\mathrm{initial}}$. Using Proposition 2, $\overline{\mathrm{SE}}_{\mathrm{SR}_1}\left(P_{\mathrm{R}_2}, x_{\mathrm{C}}\right)$ is monotonically decreasing on $x_{\mathrm{C}} = [r, \infty)$. Thus, when $\overline{\mathrm{SE}}_{\mathrm{SR}_1}\left(P_{\mathrm{R}_2}, x_{\mathrm{C}}^{\mathrm{initial}}\right) < \overline{\mathrm{SE}}_{\mathrm{R}_2\mathrm{D}}\left(P_{\mathrm{R}_2}, x_{\mathrm{C}}^{\mathrm{initial}}\right)$, the x-axial movement direction of x_{C} is determined as the negative x-axis (S-side).

Furthermore, the distance moved by x_{C} to obtain $x_{\mathrm{C}}^{\mathrm{optimal}}$ must be determined. Thus, as x_{C} moves toward S, the candidates for $x_{\mathrm{C}}^{\mathrm{optimal}}$ are explored. Herein, x_{C} was determined to be a candidate if $\overline{\mathrm{SE}}_{\mathrm{SR}_1}\left(P_{\mathrm{R}_2}, x_{\mathrm{C}}\right)$ has a local maximum or $\overline{\mathrm{SE}}_{\mathrm{SR}_1}\left(P_{\mathrm{R}_2}, x_{\mathrm{C}}\right)$ and $\overline{\mathrm{SE}}_{\mathrm{R}_2\mathrm{D}}\left(P_{\mathrm{R}_2}, x_{\mathrm{C}}\right)$ have an intersection. After the completion of search process, x_{C} which has the highest $\overline{\mathrm{SE}}_{\mathrm{SD}}\left(P_{\mathrm{R}_2}, x_{\mathrm{C}}\right)$ among the candidates is determined as $x_{\mathrm{C}}^{\mathrm{optimal}}$.

3) CASE 3: $\overline{\mathrm{SE}}_{\mathrm{SR}_1}\left(P_{\mathrm{R}_2}, x_{\mathrm{C}}^{\mathrm{initial}}\right) = \overline{\mathrm{SE}}_{\mathrm{R}_2\mathrm{D}}\left(P_{\mathrm{R}_2}, x_{\mathrm{C}}^{\mathrm{initial}}\right)$

Let us assume that the x-axial movement direction of x_{C} is the positive x-axis (D-side). According to the Proposition 1, $\overline{\mathrm{SE}}_{\mathrm{SR}_1}\left(P_{\mathrm{R}_2}, x_{\mathrm{C}}\right)$ is strictly decreasing on $x_{\mathrm{C}} = [x_{\mathrm{D}}/2, \infty)$. From (5), $\overline{\mathrm{SE}}_{\mathrm{SD}}\left(P_{\mathrm{R}_2}, x_{\mathrm{C}}\right)$ is determined by the link with the lowest $\overline{\mathrm{SE}}$. Therefore, when $x_{\mathrm{C}} = (x_{\mathrm{D}}/2, \infty)$, $\overline{\mathrm{SE}}_{\mathrm{SD}}\left(P_{\mathrm{R}_2}, x_{\mathrm{C}}\right)$ cannot be greater than $\overline{\mathrm{SE}}_{\mathrm{SD}}\left(P_{\mathrm{R}_2}, x_{\mathrm{C}}^{\mathrm{initial}}\right)$ and it is independent of the increment in $\overline{\mathrm{SE}}_{\mathrm{R}_2\mathrm{D}}\left(P_{\mathrm{R}_2}, x_{\mathrm{C}}\right)$ with $x_{\mathrm{C}} = [x_{\mathrm{D}}/2, \infty)$.

Furthermore, let us assume that the x-axial movement direction of x_{C} is the negative x-axis (S-side). According to Proposition 2, $\overline{\mathrm{SE}}_{\mathrm{R}_2\mathrm{D}}\left(P_{\mathrm{R}_2}, x_{\mathrm{C}}\right)$ is strictly increasing on $x_{\mathrm{C}} = (-\infty, x_{\mathrm{D}}/2]$. From (5), $\overline{\mathrm{SE}}_{\mathrm{SD}}\left(P_{\mathrm{R}_2}, x_{\mathrm{C}}\right)$ is determined by the link with the lowest $\overline{\mathrm{SE}}$. Therefore, when $x_{\mathrm{C}} = (-\infty, x_{\mathrm{D}}/2)$, $\overline{\mathrm{SE}}_{\mathrm{SD}}\left(P_{\mathrm{R}_2}, x_{\mathrm{C}}\right)$ cannot be greater than $\overline{\mathrm{SE}}_{\mathrm{SD}}\left(P_{\mathrm{R}_2}, x_{\mathrm{C}}^{\mathrm{initial}}\right)$ and it is independent of the decrement in $\overline{\mathrm{SE}}_{\mathrm{SR}_1}\left(P_{\mathrm{R}_2}, x_{\mathrm{C}}\right)$ with $x_{\mathrm{C}} = (-\infty, x_{\mathrm{D}}/2]$. Finally, we can conclude that $x_{\mathrm{C}}^{\mathrm{initial}}$ is $x_{\mathrm{C}}^{\mathrm{optimal}}$.

4) A PSEUDO CODE FOR THE PROPOSED ALGORITHM

Algorithm 1 describes the pseudo code for the proposed center point adjustment method. If $\overline{\mathrm{SE}}_{\mathrm{SR}_1}\left(P_{\mathrm{R}_2}, x_{\mathrm{C}}^{\mathrm{initial}}\right) > \overline{\mathrm{SE}}_{\mathrm{R}_2\mathrm{D}}\left(P_{\mathrm{R}_2}, x_{\mathrm{C}}^{\mathrm{initial}}\right)$ (line 1), x_{C} moves toward D as $x_{\mathrm{C}} \leftarrow x_{\mathrm{C}} + \Delta x$ (line 9). Herein, if $x_{\mathrm{C}} = [x_{\mathrm{D}}, \infty)$, x_{C} becomes stationary and the loop ends (lines 6-8) because according to Proposition 1, $\overline{\mathrm{SE}}_{\mathrm{SD}}\left(P_{\mathrm{R}_2}, x_{\mathrm{C}}\right)$ is monotonically decreasing on $x_{\mathrm{C}} = [x_{\mathrm{D}}, \infty)$ as $\overline{\mathrm{SE}}_{\mathrm{SR}_1}\left(P_{\mathrm{R}_2}, x_{\mathrm{C}}\right)$ is strictly decreasing on $x_{\mathrm{C}} = [x_{\mathrm{D}}, \infty)$ and $\overline{\mathrm{SE}}_{\mathrm{R}_2\mathrm{D}}\left(P_{\mathrm{R}_2}, x_{\mathrm{C}}\right)$ is monotonically decreasing on $x_{\mathrm{C}} = [x_{\mathrm{D}}, \infty)$ (see the graph when $x_{\mathrm{C}} \geq$ 1300m in Fig. 3). If x_{C} attains the local maximum of $\overline{\mathrm{SE}}_{\mathrm{R}_2\mathrm{D}}\left(P_{\mathrm{R}_2}, x_{\mathrm{C}}\right)$ while moving toward D (line 3), the corresponding x_{C} is inserted into set $\mathcal{A}$ (line 4). Additionally, if x_{C} attains $x_{\mathrm{C}}^{\mathrm{intersection}}$ that denotes the x-coordinate of the intersection between $\overline{\mathrm{SE}}_{\mathrm{R}_2\mathrm{D}}\left(P_{\mathrm{R}_2}, x_{\mathrm{C}}\right)$ and $\overline{\mathrm{SE}}_{\mathrm{SR}_1}\left(P_{\mathrm{R}_2}, x_{\mathrm{C}}\right)$ while moving toward D (line 10), the corresponding x_{C} is inserted into set $\mathcal{A}$ (line 11). Herein, x_{C} becomes stationary (line 12). According to Proposition 1, $\overline{\mathrm{SE}}_{\mathrm{SR}_1}\left(P_{\mathrm{R}_2}, x_{\mathrm{C}}\right)$ is strictly decreasing on $x_{\mathrm{C}} = [x_{\mathrm{D}}/2, \infty)$. Since $x_{\mathrm{D}}/2 < x_{\mathrm{C}}^{\mathrm{intersection}}$, $\overline{\mathrm{SE}}_{\mathrm{SR}_1}\left(P_{\mathrm{R}_2}, x_{\mathrm{C}}\right)$ is strictly decreasing on $x_{\mathrm{C}} = [x_{\mathrm{C}}^{\mathrm{intersection}}, \infty)$. Thus, after attaining $x_{\mathrm{C}}^{\mathrm{intersection}}$, $\overline{\mathrm{SE}}_{\mathrm{SD}}\left(P_{\mathrm{R}_2}, x_{\mathrm{C}}\right)$ cannot be greater than $\overline{\mathrm{SE}}_{\mathrm{SD}}\left(P_{\mathrm{R}_2}, x_{\mathrm{C}}^{\mathrm{intersection}}\right)$ as $\overline{\mathrm{SE}}_{\mathrm{SR}_1}\left(P_{\mathrm{R}_2}, x_{\mathrm{C}}\right)$ is decreasing on $x_{\mathrm{C}} = [x_{\mathrm{C}}^{\mathrm{intersection}}, \infty)$, independent of the increment in $\overline{\mathrm{SE}}_{\mathrm{R}_2\mathrm{D}}\left(P_{\mathrm{R}_2}, x_{\mathrm{C}}\right)$ on $x_{\mathrm{C}} = [x_{\mathrm{C}}^{\mathrm{intersection}}, \infty)$ (see the graph after the intersection in Fig. 3 (b) and the first intersection in Fig. 3 (c)).

If $\overline{\mathrm{SE}}_{\mathrm{SR}_1}\left(P_{\mathrm{R}_2}, x_{\mathrm{C}}^{\mathrm{initial}}\right) < \overline{\mathrm{SE}}_{\mathrm{R}_2\mathrm{D}}\left(P_{\mathrm{R}_2}, x_{\mathrm{C}}^{\mathrm{initial}}\right)$ (line 15), x_{C} moves toward S as $x_{\mathrm{C}} \leftarrow x_{\mathrm{C}} - \Delta x$ (line 23). Herein, if $x_{\mathrm{C}} = (-\infty, 0]$, x_{C} becomes stationary and the loop ends (lines 20–22) because according to Proposition 2, $\overline{\mathrm{SE}}_{\mathrm{SD}}\left(P_{\mathrm{R}_2}, x_{\mathrm{C}}\right)$ is monotonically increasing on $x_{\mathrm{C}} = (-\infty, 0]$ as $\overline{\mathrm{SE}}_{\mathrm{SR}_1}\left(P_{\mathrm{R}_2}, x_{\mathrm{C}}\right)$ is monotonically increasing on

Algorithm 1 Center Point Adjustment Algorithm

1: **if** $\overline{\mathrm{SE}}_{\mathrm{SR}_1}\left(P_{\mathrm{R}_2}, x_{\mathrm{C}}^{\mathrm{initial}}\right) > \overline{\mathrm{SE}}_{\mathrm{R}_2\mathrm{D}}\left(P_{\mathrm{R}_2}, x_{\mathrm{C}}^{\mathrm{initial}}\right)$ **then**
2: **while** $x_{\mathrm{C}} \leq x_{\mathrm{D}}$ **do**
3: **if** x_{C} is a local maximum point of $\overline{\mathrm{SE}}_{\mathrm{R}_2\mathrm{D}}\left(P_{\mathrm{R}_2}, x_{\mathrm{C}}\right)$ **then**
4: insert x_{C} in $\mathcal{A}$
5: **end if**
6: **if** $x_{\mathrm{C}} = x_{\mathrm{D}}$
7: break
8: **end if**
9: $x_{\mathrm{C}} \leftarrow x_{\mathrm{C}} + \Delta x$
10: **if** $x_{\mathrm{C}} = x_{\mathrm{C}}^{\mathrm{intersection}}$ **then**
11: insert x_{C} in $\mathcal{A}$
12: break
13: **end if**
14: **end while**
15: **else if** $\overline{\mathrm{SE}}_{\mathrm{SR}_1}\left(P_{\mathrm{R}_2}, x_{\mathrm{C}}^{\mathrm{initial}}\right) < \overline{\mathrm{SE}}_{\mathrm{R}_2\mathrm{D}}\left(P_{\mathrm{R}_2}, x_{\mathrm{C}}^{\mathrm{initial}}\right)$ **then**
16: **while** $x_{\mathrm{C}} \geq 0$ **do**
17: **if** x_{C} is a local maximum point of $\overline{\mathrm{SE}}_{\mathrm{SR}_1}\left(P_{\mathrm{R}_2}, x_{\mathrm{C}}\right)$ **then**
18: insert x_{C} in $\mathcal{A}$
19: **end if**
20: **if** $x_{\mathrm{C}} = 0$
21: break
22: **end if**
23: $x_{\mathrm{C}} \leftarrow x_{\mathrm{C}} - \Delta x$
24: **if** $x_{\mathrm{C}} = x_{\mathrm{C}}^{\mathrm{intersection}}$ **then**
25: insert x_{C} in $\mathcal{A}$
26: break
27: **end if**
28: **end while**
29: **else**
30: insert x_{C} in $\mathcal{A}$
31: **end if**
32: $x_{\mathrm{C}}^{\mathrm{optimal}} \leftarrow \underset{i \in A}{\mathrm{argmax}} \left(\min\left(\overline{\mathrm{SE}}_{\mathrm{SR}_1}\left(P_{\mathrm{R}_2}, i\right), \overline{\mathrm{SE}}_{\mathrm{R}_2\mathrm{D}}\left(P_{\mathrm{R}_2}, i\right)\right)\right)$

$x_C = (-\infty, 0]$ and $\overline{SE}_{R_2D}(P_{R_2}, x_C)$ is strictly increasing on $x_C = (-\infty, 0]$. If x_C attains the local maximum of $\overline{SE}_{SR_1}(P_{R_2}, x_C)$ while moving toward S (line 17), the corresponding x_C is inserted into set $\mathcal{A}$ (line 18). Additionally, if x_C attains $x_C^{\text{intersection}}$ while moving toward S (line 24), the corresponding x_C is inserted into set $\mathcal{A}$ (line 25). Herein, x_C becomes stationary (line 26). According to Proposition 2, $\overline{SE}_{R_2D}(P_{R_2}, x_C)$ is strictly increasing on $x_C = (-\infty, x_D/2]$. Since $x_C^{\text{intersection}} < x_D/2$, $\overline{SE}_{R_2D}(P_{R_2}, x_C)$ is strictly increasing on $x_C = (-\infty, x_C^{\text{intersection}}]$. Thus, after attaining $x_C^{\text{intersection}}$, $\overline{SE}_{SD}(P_{R_2}, x_C)$ cannot be greater than $\overline{SE}_{SD}(P_{R_2}, x_C^{\text{intersection}})$ as $\overline{SE}_{R_2D}(P_{R_2}, x_C)$ is increasing on $x_C = (-\infty, x_C^{\text{intersection}}]$ independent of the decrement in $\overline{SE}_{SR_1}(P_{R_2}, x_C)$ on $x_C = (-\infty, x_C^{\text{intersection}}]$.

If $\overline{SE}_{SR_1}(P_{R_2}, x_C^{\text{initial}}) = \overline{SE}_{R_2D}(P_{R_2}, x_C^{\text{initial}})$ (line 29), x_C^{initial} coincides with x_C^{optimal}. Thus, x_C^{initial} is inserted into set $\mathcal{A}$ (line 30).

After the search process completes, the x_C with the highest $\overline{SE}_{SD}(P_{R_2}, x_C)$ among the candidates in set $\mathcal{A}$ is determined as x_C^{optimal} (line 32).

B. TRANSMIT POWER ADJUSTMENT ALGORITHM

In this subsection, a transmission power adjustment algorithm is proposed to improve $\overline{SE}_{SD}$. Particularly, R_2 denotes the UAV transmitting data within the $\{R \rightarrow D\}$ section; thus, the UAV's transmission power is denoted as P_{R_2}. We assume that x_C is given and the transmission power of UAV is not greater than that of S ($P_{R_2} \leq P_S$) [31]. The initial P_{R_2} is denoted as $P_{R_2}^{\text{initial}}$. To enhance $\overline{SE}_{SD}(P_{R_2}, x_C)$, the initial performance of each link, i.e., $\overline{SE}_{SR_1}(P_{R_2}^{\text{initial}}, x_C)$ and $\overline{SE}_{R_2D}(P_{R_2}^{\text{initial}}, x_C)$, is compared and P_{R_2} is adjusted according to the comparison results. In each case, we use the following proposition.

Proposition 3: $\overline{SE}_{R_2D}(P_{R_2}, x_C)$ is strictly increasing on $P_{R_2} = [0, \infty)$ and $\overline{SE}_{SR_1}(P_{R_2}, x_C)$ is strictly decreasing on $P_{R_2} = [0, \infty)$.

Proof: See Appendix C.

Henceforth, we describe the adjustment of P_{R_2} to determine the optimal $P_{R_2}(P_{R_2}^{\text{optimal}})$ that enhances $\overline{SE}_{SD}(P_{R_2}, x_C)$ in each case.

1) CASE 1: $\overline{SE}_{SR_1}(P_{R_2}^{\text{initial}}, x_C) > \overline{SE}_{R_2D}(P_{R_2}^{\text{initial}}, x_C)$

From (5), $\overline{SE}_{SD}(P_{R_2}, x_C)$ is determined by the link having the lowest $\overline{SE}$. Thus, $\overline{SE}_{SD}(P_{R_2}, x_C)$ increases as the minimum value between $\overline{SE}_{SR_1}(P_{R_2}, x_C)$ and $\overline{SE}_{R_2D}(P_{R_2}, x_C)$ increases. From Proposition 3, $\overline{SE}_{R_2D}(P_{R_2}, x_C)$ is strictly increasing on $P_{R_2} = [0, \infty)$. Thus, in this case, we increase P_{R_2} in order to increase $\overline{SE}_{SD}(P_{R_2}, x_C)$.

Based on Proposition 3, if there is an intersection between $\overline{SE}_{SR_1}(P_{R_2}, x_C)$ and $\overline{SE}_{R_2D}(P_{R_2}, x_C)$ while increasing P_{R_2}, then P_{R_2} such that $\overline{SE}_{SR_1}(P_{R_2}, x_C)$ and $\overline{SE}_{R_2D}(P_{R_2}, x_C)$ have an intersection is $P_{R_2}^{\text{optimal}}$ (see Fig. 4 (a)). Therefore, the intersection point is discovered while increasing P_{R_2}. If there is no intersection between $\overline{SE}_{SR_1}(P_{R_2}, x_C)$ and $\overline{SE}_{R_2D}(P_{R_2}, x_C)$ while increasing P_{R_2}, $P_{R_2}^{\max}$ that denotes the maximum P_{R_2} coincides with $P_{R_2}^{\text{optimal}}$ (see Fig. 4 (b)).

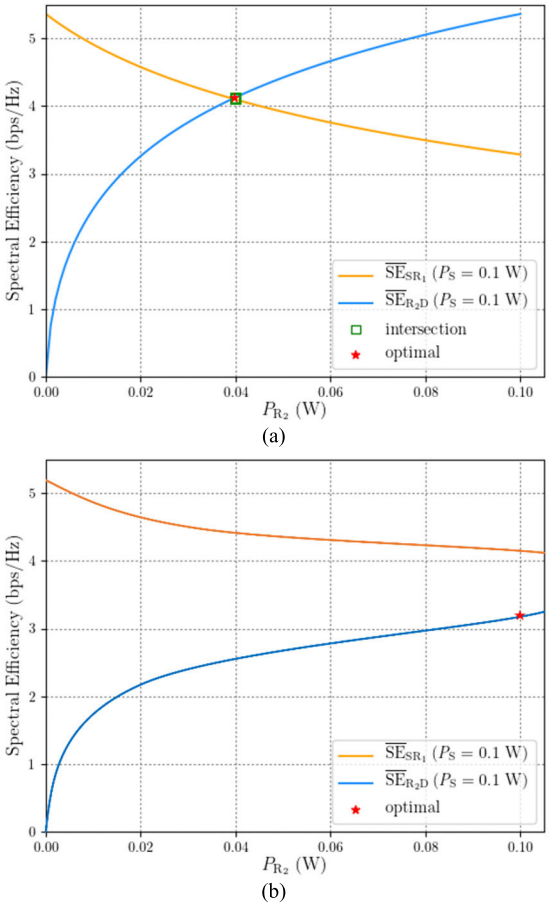

FIGURE 4. Examples of $\overline{SE}_{SR_1}$ and $\overline{SE}_{R_2D}$ when $\overline{SE}_{SR_1}(P_{R_2}^{\text{initial}}, x_C) > \overline{SE}_{R_2D}(P_{R_2}^{\text{initial}}, x_C)$. (a) The case that an intersection exists. (b) The case that an intersection does not exist.

2) CASE 2: $\overline{SE}_{SR_1}(P_{R_2}^{\text{initial}}, x_C) < \overline{SE}_{R_2D}(P_{R_2}^{\text{initial}}, x_C)$

From (5), $\overline{SE}_{SD}(P_{R_2}, x_C)$ is determined by the link having the lowest $\overline{SE}$. Thus, $\overline{SE}_{SD}(P_{R_2}, x_C)$ increases as the minimum value between $\overline{SE}_{SR_1}(P_{R_2}, x_C)$ and $\overline{SE}_{R_2D}(P_{R_2}, x_C)$ increases. Using Proposition 3, $\overline{SE}_{SR_1}(P_{R_2}, x_C)$ is strictly decreasing on $P_{R_2} = [0, \infty)$. Thus, in this case, we decrease P_{R_2} in order to increase $\overline{SE}_{SD}(P_{R_2}, x_C)$.

From Proposition 3, if there is an intersection between $\overline{SE}_{SR_1}(P_{R_2}, x_C)$ and $\overline{SE}_{R_2D}(P_{R_2}, x_C)$ while decreasing P_{R_2}, then P_{R_2} such that $\overline{SE}_{SR_1}(P_{R_2}, x_C)$ and $\overline{SE}_{R_2D}(P_{R_2}, x_C)$ have an intersection is $P_{R_2}^{\text{optimal}}$.

Proposition 4: When $\overline{SE}_{SR_1}(P_{R_2}^{\text{initial}}, x_C) < \overline{SE}_{R_2D}(P_{R_2}^{\text{initial}}, x_C)$, an intersection between $\overline{SE}_{SR_1}(P_{R_2}, x_C)$ and $\overline{SE}_{R_2D}(P_{R_2}, x_C)$ always exists on $P_{R_2} = [0, P_{R_2}^{\text{initial}})$.

Proof: Because of $P_{R_2} \leq P_S$ constraint, if we assume that $P_{R_2} = 0$, we have $P_S \geq 0$. From (3) and (4), when

$P_{R_2} = 0$, we have $\overline{SE}_{R_2D}(P_{R_2}, x_C) = 0$ and when $P_S \geq 0$, we have $\overline{SE}_{SR_1}(P_{R_2}, x_C) \geq 0$. Thus, when $P_{R_2} = 0$, we have $\overline{SE}_{SR_1}(P_{R_2}, x_C) \geq \overline{SE}_{R_2D}(P_{R_2}, x_C)$. Finally, when $\overline{SE}_{SR_1}\left(P_{R_2}^{initial}, x_C\right) < \overline{SE}_{R_2D}\left(P_{R_2}^{initial}, x_C\right)$, an intersection between $\overline{SE}_{SR_1}(P_{R_2}, x_C)$ and $\overline{SE}_{R_2D}(P_{R_2}, x_C)$ always exists on $P_{R_2} = [0, P_{R_2}^{initial})$.

Using Proposition 4, an intersection between $\overline{SE}_{SR_1}(P_{R_2}, x_C)$ and $\overline{SE}_{R_2D}(P_{R_2}, x_C)$ always exists on $P_{R_2} = [0, P_{R_2}^{initial})$. Hence, P_{R_2} such that $\overline{SE}_{SR_1}(P_{R_2}, x_C)$ and $\overline{SE}_{R_2D}(P_{R_2}, x_C)$ have an intersection is $P_{R_2}^{optimal}$ and $P_{R_2}^{optimal}$ always exists on $P_{R_2} = [0, P_{R_2}^{initial})$.

3) CASE 3: $\overline{SE}_{SR_1}\left(P_{R_2}^{initial}, x_C\right) = \overline{SE}_{R_2D}\left(P_{R_2}^{initial}, x_C\right)$

Let us assume that P_{R_2} increases ($P_{R_2} \geq P_{R_2}^{initial}$). According to Proposition 3, $\overline{SE}_{SR_1}(P_{R_2}, x_C)$ is strictly decreasing on $P_{R_2} = [0, \infty)$ and $\overline{SE}_{R_2D}(P_{R_2}, x_C)$ is strictly increasing on $P_{R_2} = [0, \infty)$. Because $\overline{SE}_{SD}(P_{R_2}, x_C)$ is determined by the link having the lowest $\overline{SE}$, $\overline{SE}_{SD}(P_{R_2}, x_C)$ is strictly decreasing on $P_{R_2} = [P_{R_2}^{initial}, \infty)$. Therefore, when $P_{R_2} = (P_{R_2}^{initial}, \infty)$, $\overline{SE}_{SD}(P_{R_2}, x_C)$ cannot be greater than $\overline{SE}_{SD}\left(P_{R_2}^{initial}, x_C\right)$.

Furthermore, let us assume that P_{R_2} decreases ($P_{R_2} \leq P_{R_2}^{initial}$). According to Proposition 3, $\overline{SE}_{SR_1}(P_{R_2}, x_C)$ is strictly decreasing on $P_{R_2} = [0, \infty)$ and $\overline{SE}_{R_2D}(P_{R_2}, x_C)$ is strictly increasing on $P_{R_2} = [0, \infty)$. Because $\overline{SE}_{SD}(P_{R_2}, x_C)$ is determined by the link having the lowest $\overline{SE}$, $\overline{SE}_{SD}(P_{R_2}, x_C)$ is strictly increasing on $P_{R_2} = [0, P_{R_2}^{initial}]$. Therefore, when $P_{R_2} = [0, P_{R_2}^{initial})$, $\overline{SE}_{SD}(P_{R_2}, x_C)$ cannot be greater than $\overline{SE}_{SD}\left(P_{R_2}^{initial}, x_C\right)$. Finally, we can conclude that $P_{R_2}^{initial}$ is $P_{R_2}^{optimal}$.

4) A PSEUDO CODE FOR THE PROPOSED ALGORITHM

Algorithm 2 represents the pseudo code for the proposed transmit power adjustment method. If $\overline{SE}_{SR_1}\left(P_{R_2}^{initial}, x_C\right) > \overline{SE}_{R_2D}\left(P_{R_2}^{initial}, x_C\right)$ (line 1), P_{R_2} increases as $P_{R_2} \leftarrow P_{R_2} + \Delta P_{R_2}$ in order to increase $\overline{SE}_{SD}(P_{R_2}, x_C)$ (line 3). According to the transmit power constraint of the UAV ($P_{R_2} \leq P_S$), the increase in P_{R_2} is considered on $P_{R_2} = [P_{R_2}^{initial}, P_S]$ (line 2). Let $P_{R_2}^{intersection}$ denote P_{R_2} such that $\overline{SE}_{SR_1}(P_{R_2}, x_C)$ and $\overline{SE}_{R_2D}(P_{R_2}, x_C)$ intersect. If P_{R_2} attains $P_{R_2}^{intersection}$ while increasing P_{R_2} (line 4), the loop ends because $P_{R_2}^{intersection}$ is $P_{R_2}^{optimal}$ (line 5). After the loop ends, the current P_{R_2} is determined as $P_{R_2}^{optimal}$ (line 8).

If $\overline{SE}_{SR_1}\left(P_{R_2}^{initial}, x_C\right) < \overline{SE}_{R_2D}\left(P_{R_2}^{initial}, x_C\right)$ (line 9), P_{R_2} decreases as $P_{R_2} \leftarrow P_{R_2} - \Delta P_{R_2}$ in order to increase $\overline{SE}_{SD}(P_{R_2}, x_C)$ (line 11). Herein, the decrease in P_{R_2} is considered on $P_{R_2} = [0, P_{R_2}^{initial}]$ (line 10). If P_{R_2} attains $P_{R_2}^{intersection}$ while decreasing P_{R_2} (line 12), the loop ends (line 13). After the loop ends, the current P_{R_2} is determined as $P_{R_2}^{optimal}$ (line 16).

Algorithm 2 Transmission Power Adjustment Algorithm

1: **if** $\overline{SE}_{SR_1}\left(P_{R_2}^{initial}, x_C\right) > \overline{SE}_{R_2D}\left(P_{R_2}^{initial}, x_C\right)$ **then**
2: **while** $P_{R_2} \leq P_S$ **do**
3: $P_{R_2} \leftarrow P_{R_2} + \Delta P_{R_2}$
4: **if** $P_{R_2} = P_{R_2}^{intersection}$ **then**
5: break
6: **end if**
7: **end while**
8: $P_{R_2}^{optimal} \leftarrow P_{R_2}$
9: **else if** $\overline{SE}_{SR_1}\left(P_{R_2}^{initial}, x_C\right) < \overline{SE}_{R_2D}\left(P_{R_2}^{initial}, x_C\right)$ **then**
10: **while** $P_{R_2} \geq 0$ **do**
11: $P_{R_2} \leftarrow P_{R_2} - \Delta P_{R_2}$
12: **if** $P_{R_2} = P_{R_2}^{intersection}$ **then**
13: break
14: **end if**
15: **end while**
16: $P_{R_2}^{optimal} \leftarrow P_{R_2}$
17: **else**
18: $P_{R_2}^{optimal} \leftarrow P_{R_2}$
19: **end if**

TABLE 2. Simulation parameters.

Parameter	Value
x_D	400~1600 m
P_S	0.1 W
P_{R_2}	0.025 W
x_C	$x_D/2$
β	-60 dB
σ^2	-110 dBm
α	2

If $\overline{SE}_{SR_1}\left(P_{R_2}^{initial}, x_C\right) = \overline{SE}_{R_2D}\left(P_{R_2}^{initial}, x_C\right)$ (line 17), the adjustment of P_{R_2} is not considered because $P_{R_2}^{initial}$ is $P_{R_2}^{optimal}$, and the current P_{R_2} is determined as $P_{R_2}^{optimal}$ (line 18).

V. SIMULATION RESULTS

In this section, we evaluate the performance of the proposed relaying scheme, center point adjustment algorithm and transmit power adjustment algorithm. The main simulation parameters are given in Table 2. The distance between S and D is assumed as 400∼1600 m and denoted as x_D ($\|\mathbf{X}_S - \mathbf{X}_D\| = x_D$). The transmission power of S is assumed constant at $P_S = 0.1$ W. In Section III, UAVs close to S and D were defined as R_1 and R_2, respectively, i.e., R_2 denotes the UAV that transmits data within the {R → D} section; thus, the transmission power of the UAV is denoted as P_{R_2}. We assume that the initial transmission power of R_2

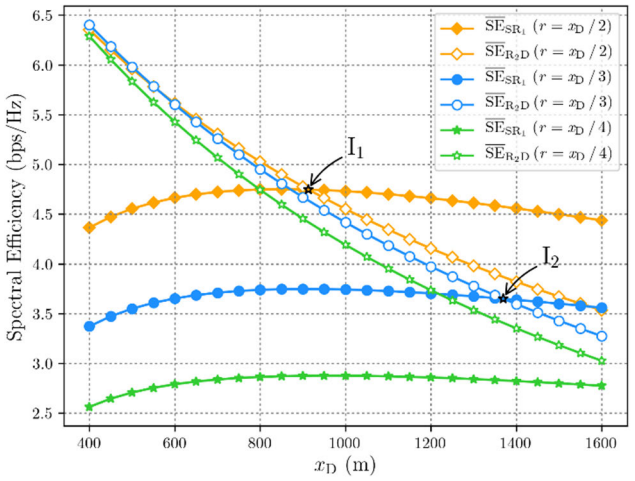

FIGURE 5. Spectral efficiency of each link with varying r and x_D.

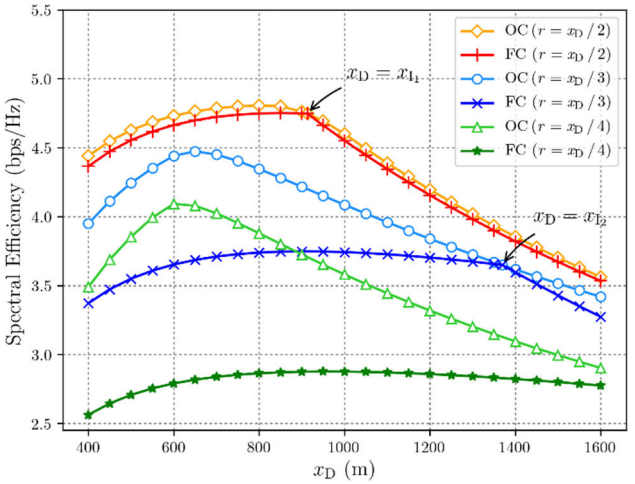

FIGURE 6. Spectral efficiency of the proposed relaying schemes with and without the center point adjustment algorithm.

is $P_{R_2} = 0.025$ W. As shown in Fig. 1, the x-coordinate of the initial center point is set to $x_C = x_D/2$. The channel gain at the reference distance is $\beta = -60$ dB and the noise power is $\sigma^2 = -110$ dBm.

Fig. 5 shows the average SE of $\{S \rightarrow R_1\}$ link $\left(\overline{SE}_{SR_1}\right)$ and the average SE of $\{R_2 \rightarrow D\}$ link $\left(\overline{SE}_{R_2D}\right)$ of the proposed relaying scheme for varying x_D and trajectory radius r. In Fig. 5, I_1 and I_2 represent the intersection points of $\overline{SE}_{SR_1}$ and $\overline{SE}_{R_2D}$ for $r = x_D/2$ and $r = x_D/3$, respectively. If the x-coordinates of intersection points I_1 and I_2 are defined as x_{I_1} and x_{I_2}, respectively, we can determine that $x_{I_1} < x_{I_2}$ because a decrease in r increases IRI, thereby causing a decrease in $\overline{SE}_{SR_1}$ based on (3a) and (4a). For $r = x_D/4$, the intersection point of $\overline{SE}_{SR_1}$ and $\overline{SE}_{R_2D}$ is not indicated in Fig. 5 because x_D only up to 1600 m was considered in this simulation. As shown in Fig. 5, each $\overline{SE}_{R_2D}$ decreases as x_D increases because the strength of the received signal at D decreases as x_D increases while P_{R_2} is fixed. Furthermore, each $\overline{SE}_{SR_1}$ increases up to a certain point and then decreases. From (3a) and (4a), it can be observed that the factors affecting $\overline{SE}_{SR_1}$ can be IRI and the strength of the received signal at R_1. As x_D increases, IRI and the strength of the received signal at R_1 decrease (in the case of IRI, the increase in x_D leads to an increase in r and which causes a decrease in IRI). A decrease in IRI causes an increase in $\overline{SE}_{SR_1}$, and a decrease in the strength of the received signal at R_1 causes a decrease in $\overline{SE}_{SR_1}$. In Fig. 5, $\overline{SE}_{SR_1}$ increases up to a certain point, indicating that IRI is the dominant factor affecting $\overline{SE}_{SR_1}$ in the corresponding range. Additionally, because $\overline{SE}_{SR_1}$ decreases after a certain point, the dominant factor affecting $\overline{SE}_{SR_1}$ is the strength of the received signal at R_1 in the corresponding range. When x_D is relatively small (i.e., below a certain point), $\overline{SE}_{SR_1}$ is greatly affected by IRI because of its large magnitude, and when x_D is relatively large (i.e., after a certain point), IRI is small and $\overline{SE}_{SR_1}$ is less affected by IRI. Despite the transmission power of S being higher than that of R_2, $\overline{SE}_{SR_1} < \overline{SE}_{R_2D}$ range always exists in all cases because, unlike $\overline{SE}_{R_2D}$, $\overline{SE}_{SR_1}$ is degraded by IRI according to (3a) and (4a).

Fig. 6 compares the average end-to-end SE $\left(\overline{SE}_{SD}\right)$ with and without the center point adjustment algorithm for varying x_D and r. For brevity, the cases with and without the center point adjustment algorithm are represented as optimized center (OC) and fixed center (FC), respectively. Our proposed center point adjustment algorithm compares $\overline{SE}_{SR_1}$ and $\overline{SE}_{R_2D}$ and moves the center point based on their comparison results to increase $\overline{SE}_{SD}$. The comparison results of $\overline{SE}_{SR_1}$ and $\overline{SE}_{R_2D}$ can be obtained from Fig. 5. For $\overline{SE}_{SR_1} < \overline{SE}_{R_2D}$, our proposed algorithm increases $\overline{SE}_{SD}$ by moving the center point toward S and for $\overline{SE}_{SR_1} > \overline{SE}_{R_2D}$, our proposed algorithm increases $\overline{SE}_{SD}$ by moving the center point toward D. For $\overline{SE}_{SR_1} = \overline{SE}_{R_2D}$, the center point is not moved because the initial center point is optimal. The arrows in Fig. 6 indicate the points at which $x_D = x_{I_1}$ and $x_D = x_{I_2}$, respectively. For $\overline{SE}_{SR_1} = \overline{SE}_{R_2D}$, the initial center point is optimal, thus it can be observed that $\overline{SE}_{SD}$ of OC and FC are the same at $x_D = x_{I_1}$ and $x_D = x_{I_2}$. Simulation result shows that OC has higher or equal performance than FC in all range of 400 m $\leq x_D \leq$ 1600 m.

Fig. 7 compares the average end-to-end SE $\left(\overline{SE}_{SD}\right)$ of optimized power (OP) case with our proposed transmit power adjustment algorithm and $\overline{SE}_{SD}$ of fixed power (FP) case without the proposed algorithm. Simulation results indicate that the performance of OP is greater than or equal to that of FP in all ranges of 400 m $\leq x_D \leq$ 1600 m. According to our proposed algorithm, $\overline{SE}_{SD}$ increases with decreasing P_{R_2} when $\overline{SE}_{SR_1} < \overline{SE}_{R_2D}$, and $\overline{SE}_{SD}$ increases with increasing P_{R_2} when $\overline{SE}_{SR_1} > \overline{SE}_{R_2D}$. The arrows in Fig. 7 indicate the points at which $x_D = x_{I_1}(x_{I_2})$. According to our proposed algorithm, $\overline{SE}_{SD}$ of OP and FP are equal when $\overline{SE}_{SR_1} = \overline{SE}_{R_2D}$ because the initial P_{R_2} is optimal P_{R_2}. Note that when $\overline{SE}_{SR_1} < \overline{SE}_{R_2D}$, our proposed algorithm increases $\overline{SE}_{SD}$ by decreasing P_{R_2}, which means that a higher performance can

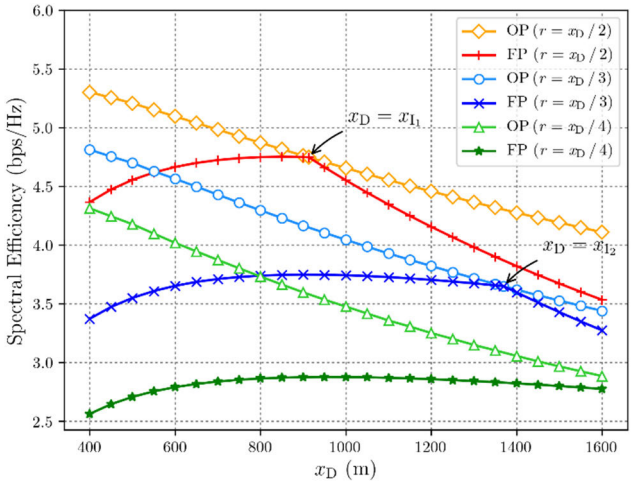

FIGURE 7. Spectral efficiency of the proposed relaying schemes with and without the transmit power adjustment algorithm.

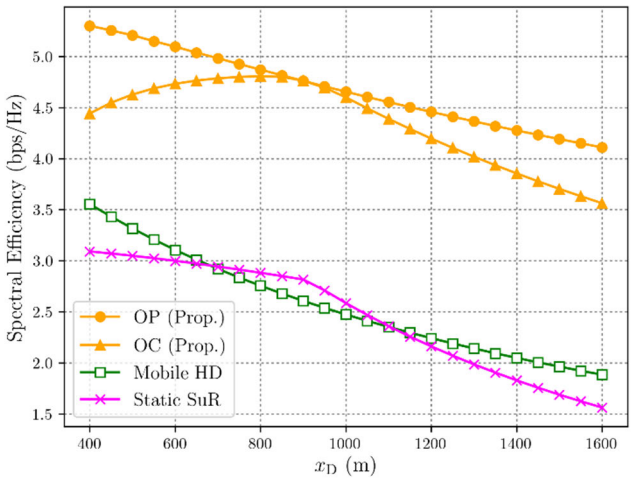

FIGURE 8. Spectral efficiency of the proposed relaying schemes versus conventional relaying schemes.

be obtained even though less transmission power is utilized. This is because when P_{R_2} is high, $\overline{SE}_{SR_1}$ decreases as IRI increases owing to (3a) and (4a). Therefore, adjusting the transmission power of this system is crucial to transmit data in an energy-efficient manner.

Fig. 8 shows the average end-to-end SE $\left(\overline{SE}_{SD}\right)$ of the proposed schemes and conventional schemes. The following are the two proposed schemes: one for adjusting the center point (OC) and the other for adjusting the transmission power (OP). It was assumed that $r = x_D/2$ for each case. The following are the two conventional schemes: mobile HD and static SuR [15], [25]. For mobile HD [25], it was assumed that one UAV operating the HD protocol follows a circular trajectory. Because this scheme optimizes the radius of the trajectory to maximize the average end-to-end SE, $\overline{SE}_{SD}$ was measured using this optimized radius. For static SuR [15], two terrestrial relays were employed. The position of each relay was set to $(x_D/2, r, 0)$ and $(x_D/2, -r, 0)$, respectively; thus, the distance between relays was $2r$. For all x_D within the given range, the proposed relaying schemes can achieve a higher SE performance compared to conventional relaying schemes. As the HD relaying scheme divides the time slots based on the {S → R} range and {R → D} range, the SE performance degrades. For static relaying, the performance is degraded by the path loss that occurs depending on the distance between the relay and target.

VI. CONCLUSION

In this study, a virtual FD relaying scheme for UAV-aided communication networks is proposed. Two UAVs moving along a circular trajectory were used as relays, and the virtual FD relaying scheme was combined with data ferry technology by utilizing the high mobility of the corresponding UAVs. Furthermore, we verified that variations in the center point of UAV trajectory and the transmission power of UAV vary the SE performance by differentiating the SNR or SINR with respect to the center point of trajectory or the transmission power. Subsequently, the center point adjustment algorithm and the transmit power adjustment algorithm were proposed, which increase the proposed relaying scheme's performance. In future work, jointly optimizing the center point of the trajectory and the transmit power of the UAV may be investigated to increase the system performance.

APPENDIXES

APPENDIX A

PROOF OF PROPOSITION 1

For convenience, the notations of variables are omitted; for instance, $\gamma_{R_2D}\left(P_{R_2}, x_C, \theta_2\right) \rightarrow \gamma_{R_2D}$, $SE_{R_2D}(P_{R_2}, x_C, \theta_2) \rightarrow SE_{R_2D}$, and $\overline{SE}_{R_2D}\left(P_{R_2}, x_C\right) \rightarrow \overline{SE}_{R_2D}$. SE_k, where $k \in \{SR_1, R_2D\}$ is a logarithmic function, i.e., $SE_k = \log_2(1+\gamma_k)$. The logarithmic function, $f = \log_a(x), (a > 1)$ is a strictly increasing function on $x = (0, \infty)$. Accordingly, SE_k is a strictly increasing function on $\gamma_k = (0, \infty)$. Henceforth, we differentiate γ_k with respect to x_C to examine the increase (or decrease) of γ_k, SE_k, and $\overline{SE}_k$.

First, using quotient rule, the differentiation of γ_{R_2D} with respect to x_C can be represented as

$$\frac{\partial}{\partial x_C}\gamma_{R_2D} = \frac{-2P_{R_2}\beta\left(x_C - x_D - r\sin\theta_2\right)}{\sigma^2\left\{(x_C - x_D - r\sin\theta_2)^2 + (r\cos\theta_2)^2 + H^2\right\}^2}, \tag{A.1}$$

where $\pi \le \theta_2 \le 2\pi$.

The maximum value of the numerator of $\partial/\partial x_C\gamma_{R_2D}$ is $-2P_{R_2}\beta\left(x_C - x_D\right)$ when $\theta_2 = 2\pi$. If the maximum value of the numerator is less than or equal to 0, then any value of the numerator is less than or equal to 0. Because the denominator of $\partial/\partial x_C\gamma_{R_2D}$ is always greater than 0, when $-2P_{R_2}\beta\left(x_C - x_D\right) \le 0$, the value of $\partial/\partial x_C\gamma_{R_2D}$ is either negative or 0. Because the derivative $\partial/\partial x_C\gamma_{R_2D}$ for $x_C \ge x_D$ is always negative or 0, γ_{R_2D} monotonically decreases on

$$\frac{\partial}{\partial P_{\mathrm{R}_2}}\gamma_{\mathrm{SR}_1}=\frac{-P_{\mathrm{S}}\beta^2}{\left[(2r)\left\{\sigma^2+P_{\mathrm{R}_2}\beta\,(2r)^{-2}\right\}\left\{(x_{\mathrm{C}}-r\sin\theta_1)^2+(r\cos\theta_1)^2+H^2\right\}\right]^2}, \tag{C.2}$$

$x_{\mathrm{C}}=[x_{\mathrm{D}},\infty)$. Hence, $\mathrm{SE}_{\mathrm{R}_2\mathrm{D}}$ monotonically decreases on $x_{\mathrm{C}}=[x_{\mathrm{D}},\infty)$ for any θ_2 within the range $[\pi,2\pi]$, and thus, $\overline{\mathrm{SE}}_{\mathrm{R}_2\mathrm{D}}$ obtained by (4b) monotonically decreases on $x_{\mathrm{C}}=[x_{\mathrm{D}},\infty)$.

In (A.1), the minimum value of the numerator of $\partial/\partial x_{\mathrm{C}}\gamma_{\mathrm{R}_2\mathrm{D}}$ is $-2P_{\mathrm{R}_2}\beta\,(x_{\mathrm{C}}-x_{\mathrm{D}}+r)$ when $\theta_2=3\pi/2$. If the minimum value of the numerator is greater than or equal to 0, then any value of the numerator is greater than or equal to 0. When $-2P_{\mathrm{R}_2}\beta\,(x_{\mathrm{C}}-x_{\mathrm{D}}+r)\geq 0$, the value of $\partial/\partial x_{\mathrm{C}}\gamma_{\mathrm{R}_2\mathrm{D}}$ is positive or 0 because the denominator of $\partial/\partial x_{\mathrm{C}}\gamma_{\mathrm{R}_2\mathrm{D}}$ is always greater than 0. Because the derivative $\partial/\partial x_{\mathrm{C}}\gamma_{\mathrm{R}_2\mathrm{D}}$ for $x_{\mathrm{C}}\leq x_{\mathrm{D}}-r$ is always positive or 0, $\gamma_{\mathrm{R}_2\mathrm{D}}$ monotonically increases on $x_{\mathrm{C}}=(-\infty,x_{\mathrm{D}}-r]$. Hence, $\mathrm{SE}_{\mathrm{R}_2\mathrm{D}}$ monotonically increases on $x_{\mathrm{C}}=(-\infty,x_{\mathrm{D}}-r]$ for any θ_2 within the range $[\pi,2\pi]$, and thus, $\overline{\mathrm{SE}}_{\mathrm{R}_2\mathrm{D}}$ obtained by (4b) monotonically increases on $x_{\mathrm{C}}=(-\infty,x_{\mathrm{D}}-r]$.

Second, using the quotient rule, the differentiation of γ_{SR_1} with respect to x_{C} can be represented as

$$\frac{\partial}{\partial x_{\mathrm{C}}}\gamma_{\mathrm{SR}_1}=\frac{-2P_{\mathrm{S}}\beta\,(x_{\mathrm{C}}-r\sin\theta_1)}{\left\{\sigma^2+P_{\mathrm{R}_2}\beta\,(2r)^{-2}\right\}\left\{(x_{\mathrm{C}}-r\sin\theta_1)^2+(r\cos\theta_1)^2+H^2\right\}^2}, \tag{A.2}$$

where $0\leq\theta_1\leq\pi$.

In (A.2), γ_{SR_1} strictly decreases on $x_{\mathrm{C}}=[r\sin\theta_1,\infty)$. When $x_{\mathrm{C}}\geq x_{\mathrm{D}}/2$, as the constraint of $r\leq x_{\mathrm{D}}/2$, $x_{\mathrm{C}}\geq r\sin\theta_1$ independent of θ_1, and thus, γ_{SR_1} strictly decreases. Hence, $\mathrm{SE}_{\mathrm{SR}_1}$ strictly decreases on $x_{\mathrm{C}}=[x_{\mathrm{D}}/2,\infty)$ for any θ_1 within the range $[0,\pi]$, and thus, $\overline{\mathrm{SE}}_{\mathrm{SR}_1}$ obtained by (4a) strictly decreases on $x_{\mathrm{C}}=[x_{\mathrm{D}}/2,\infty)$. ■

APPENDIX B
PROOF OF PROPOSITION 2

For convenience, the notations of variables are omitted, e.g., $\gamma_{\mathrm{SR}_1}(P_{\mathrm{R}_2},x_{\mathrm{C}},\theta_1)\rightarrow\gamma_{\mathrm{SR}_1}$, $\mathrm{SE}_{\mathrm{SR}_1}(P_{\mathrm{R}_2},x_{\mathrm{C}},\theta_1)\rightarrow\mathrm{SE}_{\mathrm{SR}_1}$, and $\overline{\mathrm{SE}}_{\mathrm{SR}_1}(P_{\mathrm{R}_2},x_{\mathrm{C}})\rightarrow\overline{\mathrm{SE}}_{\mathrm{SR}_1}$. Additionally, the information mentioned in Appendix A has been omitted. From (A.2), if θ_1 is within the corresponding range, the maximum and minimum values of the numerator of $\partial/\partial x_{\mathrm{C}}\gamma_{\mathrm{SR}_1}$ are $-2P_{\mathrm{S}}\beta\,(x_{\mathrm{C}}-r)$ when $\theta_1=\pi/2$ and $-2P_{\mathrm{S}}\beta x_{\mathrm{C}}$ when $\theta_1=0$, respectively. If the maximum value of the numerator of $\partial/\partial x_{\mathrm{C}}\gamma_{\mathrm{SR}_1}$ is smaller than or equal to 0, then any value of the numerator is less than or equal to 0. The denominator of $\partial/\partial x_{\mathrm{C}}\gamma_{\mathrm{SR}_1}$ is greater than 0; thus, when $-2P_{\mathrm{S}}\beta\,(x_{\mathrm{C}}-r)\leq 0$, $\partial/\partial x_{\mathrm{C}}\gamma_{\mathrm{SR}_1}$ is negative or 0. Accordingly, when $x_{\mathrm{C}}\geq r$, γ_{SR_1} monotonically decreases. Thus, $\overline{\mathrm{SE}}_{\mathrm{SR}_1}$ monotonically decreases on $x_{\mathrm{C}}=[r,\infty)$.

If the minimum value of the numerator of $\partial/\partial x_{\mathrm{C}}\gamma_{\mathrm{SR}_1}$ is greater than or equal to 0, any value of the numerator is greater than or equal to 0. When $-2P_{\mathrm{S}}\beta x_{\mathrm{C}}\geq 0$, the value of $\partial/\partial x_{\mathrm{C}}\gamma_{\mathrm{SR}_1}$ is positive or 0, because the denominator of $\partial/\partial x_{\mathrm{C}}\gamma_{\mathrm{SR}_1}$ is greater than 0. Accordingly, when $x_{\mathrm{C}}\leq 0$, γ_{SR_1} monotonically increases. Thus, $\overline{\mathrm{SE}}_{\mathrm{SR}_1}$ monotonically increases on $x_{\mathrm{C}}=(-\infty,0]$.

From (A.1), $\gamma_{\mathrm{R}_2\mathrm{D}}$ strictly increases on $(-\infty,x_{\mathrm{D}}+r\sin\theta_2]$. When $x_{\mathrm{C}}\leq x_{\mathrm{D}}/2$, as the constraint of $r\leq x_{\mathrm{D}}/2$, $x_{\mathrm{C}}\leq x_{\mathrm{D}}+r\sin\theta_2$ independent of θ_2, and thus, $\gamma_{\mathrm{R}_2\mathrm{D}}$ strictly increases. Therefore, $\overline{\mathrm{SE}}_{\mathrm{R}_2\mathrm{D}}$ strictly increases on $x_{\mathrm{C}}=(-\infty,x_{\mathrm{D}}/2]$. ■

APPENDIX C
PROOF OF PROPOSITION 3

For convenience, the notation of variables is omitted; for instance, $\gamma_{\mathrm{SR}_1}(P_{\mathrm{R}_2},x_{\mathrm{C}},\theta_1)\rightarrow\gamma_{\mathrm{SR}_1}$, $\mathrm{SE}_{\mathrm{SR}_1}(P_{\mathrm{R}_2},x_{\mathrm{C}},\theta_1)\rightarrow\mathrm{SE}_{\mathrm{SR}_1}$, and $\overline{\mathrm{SE}}_{\mathrm{SR}_1}(P_{\mathrm{R}_2},x_{\mathrm{C}})\rightarrow\overline{\mathrm{SE}}_{\mathrm{SR}_1}$. First, we differentiate $\gamma_{\mathrm{R}_2\mathrm{D}}$ with respect to P_{R_2} to examine the increase (or decrease) of $\gamma_{\mathrm{R}_2\mathrm{D}}$, $\mathrm{SE}_{\mathrm{R}_2\mathrm{D}}$, and $\overline{\mathrm{SE}}_{\mathrm{R}_2\mathrm{D}}$. The differentiation of $\gamma_{\mathrm{R}_2\mathrm{D}}$ with respect to P_{R_2} can be represented as

$$\frac{\partial}{\partial P_{\mathrm{R}_2}}\gamma_{\mathrm{R}_2\mathrm{D}}=\frac{\beta}{\sigma^2\left\{(x_{\mathrm{C}}-x_{\mathrm{D}}-r\sin\theta_2)^2+(r\cos\theta_2)^2+H^2\right\}^2}, \tag{C.1}$$

where $\pi\leq\theta_2\leq 2\pi$.

Because the derivative $\partial/\partial P_{\mathrm{R}_2}\gamma_{\mathrm{R}_2\mathrm{D}}$ is always greater than 0, $\gamma_{\mathrm{R}_2\mathrm{D}}$ strictly increases on $P_{\mathrm{R}_2}=[0,\infty)$. Hence, $\mathrm{SE}_{\mathrm{R}_2\mathrm{D}}$ strictly increases on $P_{\mathrm{R}_2}=[0,\infty)$ for any θ_2 within the range $[\pi,2\pi]$, and thus, $\overline{\mathrm{SE}}_{\mathrm{R}_2\mathrm{D}}$ obtained by (4b) strictly increases on $P_{\mathrm{R}_2}=[0,\infty)$.

Second, we differentiate γ_{SR_1} with respect to P_{R_2} to examine the increase (or decrease) of γ_{SR_1}, $\mathrm{SE}_{\mathrm{SR}_1}$, and $\overline{\mathrm{SE}}_{\mathrm{SR}_1}$. Using the quotient rule, the differentiation of γ_{SR_1} with respect to P_{R_2} can be represented as (C2), shown at the top of the page, where $0\leq\theta_1\leq\pi$.

Because the derivative $\partial/\partial P_{\mathrm{R}_2}\gamma_{\mathrm{SR}_1}$ is always less than 0, γ_{SR_1} strictly decreases on $P_{\mathrm{R}_2}=[0,\infty)$. Hence, $\mathrm{SE}_{\mathrm{SR}_1}$ strictly decreases on $P_{\mathrm{R}_2}=[0,\infty)$ for any θ_1 within the range $[0,\pi]$, and thus, $\overline{\mathrm{SE}}_{\mathrm{SR}_1}$ obtained by (4a) strictly decreases on $P_{\mathrm{R}_2}=[0,\infty)$. ■

REFERENCES

[1] R. Kumar and A. Hossain, "Survey on half- and full-duplex relay based cooperative communications and its potential challenges and open issues using Markov chains," *IET Commun.*, vol. 13, no. 11, pp. 1537–1550, Jul. 2019.
[2] H. Murata, A. Kuwabara, and Y. Oishi, "Distributed cooperative relaying based on space-time block code: System description and measurement campaign," *IEEE Access*, vol. 9, pp. 25623–25631, 2021.
[3] L. Kong, L. Ye, F. Wu, M. Tao, G. Chen, and A. V. Vasilakos, "Autonomous relay for millimeter-wave wireless communications," *IEEE J. Sel. Areas Commun.*, vol. 35, no. 9, pp. 2127–2136, Sep. 2017.

[4] M. S. AbuZeid, Y. A. Fahmy, and M. S. El-Soudani, "Adaptive combined channel-network coding for cooperative relay aided cognitive radio networks," *Information*, vol. 12, no. 8, p. 320, Aug. 2021.
[5] E. Fidan and O. Kucur, "Performance of relay selection for NOMA based cooperative networks over shadowed fading channels," *IEEE Trans. Veh. Technol.*, vol. 70, no. 4, pp. 3283–3297, Apr. 2021.
[6] C. V. Anamuro, N. Varsier, J. Schwoerer, and X. Lagrange, "Distance-aware relay selection in an energy-efficient discovery protocol for 5G D2D communication," *IEEE Trans. Wireless Commun.*, vol. 20, no. 7, pp. 4379–4391, Jul. 2021.
[7] A. Bletsas, A. Khisti, D. P. Reed, and A. Lippman, "A simple cooperative diversity method based on network path selection," *IEEE J. Sel. Areas Commun.*, vol. 24, no. 3, pp. 659–672, Mar. 2006.
[8] A. Ikhlef, D. S. Michalopoulos, and R. Schober, "Max-max relay selection for relays with buffers," *IEEE Trans. Wireless Commun.*, vol. 11, no. 3, pp. 1124–1135, Mar. 2012.
[9] I. Krikidis, T. Charalambous, and J. S. Thompson, "Buffer-aided relay selection for cooperative diversity systems without delay constraints," *IEEE Trans. Wireless Commun.*, vol. 11, no. 5, pp. 1957–1967, May 2012.
[10] M. Duarte, C. Dick, and A. Sabharwal, "Experiment-driven characterization of full-duplex wireless systems," *IEEE Trans. Wireless Commun.*, vol. 11, no. 12, pp. 4296–4307, Dec. 2012.
[11] E. Everett, A. Sahai, and A. Sabharwal, "Passive self-interference suppression for full-duplex infrastructure nodes," *IEEE Trans. Wireless Commun.*, vol. 13, no. 2, pp. 680–694, Jan. 2014.
[12] E. Ahmed and A. M. Eltawil, "All-digital self-interference cancellation technique for full-duplex systems," *IEEE Trans. Wireless Commun.*, vol. 14, no. 7, pp. 3519–3532, Jul. 2015.
[13] K.-C. Hsu, K. C.-J. Lin, and H.-Y. Wei, "Inter-client interference cancellation for full-duplex networks," in *Proc. IEEE INFOCOM*, May 2017, pp. 1–9.
[14] Q. Y. Liau, C. Y. Leow, and Z. Ding, "Physical layer security using two-path successive relaying," *Sensors*, vol. 16, no. 6, p. 846, Jun. 2016.
[15] B. Rankov and A. Wittneben, "Spectral efficient protocols for half-duplex fading relay channels," *IEEE J. Sel. Areas Commun.*, vol. 25, no. 2, pp. 379–389, Feb. 2007.
[16] A. Ikhlef, J. Kim, and R. Schober, "Mimicking full-duplex relaying using half-duplex relays with buffers," *IEEE Trans. Veh. Technol.*, vol. 61, no. 7, pp. 3025–3037, Sep. 2012.
[17] N. Nomikos, D. Vouyioukas, T. Charalambous, I. Krikidis, P. Makris, D. N. Skoutas, M. Johansson, and C. Skianis, "Joint relay-pair selection for buffer-aided successive opportunistic relaying," *Trans. Emerg. Telecommun. Technol.*, vol. 25, no. 8, pp. 823–834, Nov. 2013.
[18] F. A. Khan, Z. A. Malik, A. A. Nasir, and M. Masood, "Relay selection & power allocation for maximizing sum-throughput of a buffered relay network," *IEEE Commun. Lett.*, vol. 24, no. 6, pp. 1318–1322, Jun. 2020.
[19] H. Wang, J. Wang, G. Ding, J. Chen, Y. Li, and Z. Han, "Spectrum sharing planning for full-duplex UAV relaying systems with underlaid D2D communications," *IEEE J. Sel. Areas Commun.*, vol. 36, no. 9, pp. 1986–1999, Sep. 2018.
[20] H. Shakhatreh, A. Alenezi, A. Sawalmeh, M. Almutiry, and W. Malkawi, "Efficient placement of an aerial relay drone for throughput maximization," *Wireless Commun. Mobile Comput.*, vol. 2021, pp. 1–11, Jun. 2021.
[21] X. Liu, D. He, and H. Ding, "Throughput maximization for UAV-enabled full-duplex relay system in 5G communications," *Phys. Commun.*, vol. 32, pp. 104–111, Feb. 2019.
[22] X. Jiang, Z. Yin, Z. Wu, Z. Yang, and J. Sun, "Outage probability optimization for UAV-enabled wireless relay networks in fading channels," *Phys. Commun.*, vol. 33, pp. 35–45, Apr. 2019.
[23] W. Wang, D. He, Y. Xu, Y. Wang, and Y. Zhang, "Power allocation and successive relay selection in UAV-assisted cooperative NOMA system," in *Proc. IEEE 6th Int. Conf. Comput. Commun. (ICCC)*, Dec. 2020, pp. 723–728.
[24] C.-M. Cheng, P.-H. Hsiao, H. T. Kung, and D. Vlah, "Maximizing throughput of UAV-relaying networks with the load-carry-and-deliver paradigm," in *Proc. IEEE Wireless Commun. Netw. Conf.*, Mar. 2007, pp. 4417–4424.
[25] J. Zhang, Y. Zeng, and R. Zhang, "Spectrum and energy efficiency maximization in UAV-enabled mobile relaying," in *Proc. IEEE Int. Conf. Commun. (ICC)*, May 2017, pp. 1–6.
[26] L. Xiao, Y. Xu, D. Yang, and Y. Zeng, "Secrecy energy efficiency maximization for UAV-enabled mobile relaying," *IEEE Trans. Green Commun. Netw.*, vol. 4, no. 1, pp. 180–193, Mar. 2020.
[27] T. Shafique, H. Tabassum, and E. Hossain, "End-to-end energy-efficiency and reliability of UAV-assisted wireless data ferrying," *IEEE Trans. Commun.*, vol. 68, no. 3, pp. 1822–1837, Mar. 2020.
[28] N. Qi, M. Wang, W.-J. Wang, T. A. Tsiftsis, R. Yao, and G. Yang, "Energy efficient full-duplex UAV relaying networks under load-carry-and-delivery scheme," *IEEE Access*, vol. 8, pp. 74349–74358, 2020.
[29] J. Joung, H. L. Lee, J. Zhao, and X. Kang, "Power control method for energy efficient buffer-aided relay systems," *Energies*, vol. 12, no. 17, p. 3234, Aug. 2019.
[30] Y. Zeng, R. Zhang, and T. J. Lim, "Throughput maximization for UAV-enabled mobile relaying systems," *IEEE Trans. Commun.*, vol. 64, no. 12, pp. 4983–4996, Dec. 2016.
[31] J. Miao and Z. Zheng, "Cooperative jamming for secure UAV-enabled mobile relay system," *IEEE Access*, vol. 8, pp. 48943–48957, 2020.

DONG HYUCK WOO received the M.S. degree in computer engineering from Kwangwoon University, Seoul, South Korea, in 2021, where he is currently pursuing the Ph.D. degree. His research interests include mobile communications, relaying, UAV-aided communications, and physical layer security.

HO YOUNG HWANG (Member, IEEE) received the B.S., M.S., and Ph.D. degrees in electrical engineering and computer science from the Korea Advanced Institute of Science and Technology (KAIST), Daejeon, South Korea, in 2000, 2002, and 2008, respectively. From 2002 to 2003, he was a Guest Researcher with the Advanced Network Technologies Division, National Institute of Standards and Technology (NIST), Gaithersburg, MD, USA. From 2008 to 2010, he was a Postdoctoral Fellow with the Department of Electrical and Computer Engineering, University of Waterloo, Canada. He joined as the Faculty Member of Kwangwoon University, Seoul, South Korea, in 2010, where he is currently a Professor with the School of Computer and Information Engineering. His research interests include wireless personal and local area networks, UAV-aided communications, relaying, sensor networks, mobile communication systems, protocols, and services.